Gas-Phase Structure of a π-Allyl−Palladium Complex: Efficient Infrared Spectroscopy in a 7 T Fourier Transform Mass Spectrometer

Joost M. Bakker,[†] Thierry Besson, Joël Lemaire, Debora Scuderi, and Philippe Maître*

Laboratoire de Chimie Physique, UMR8000 Université Paris-Sud et CNRS, Faculty of Sciences, Bâtiment 350, 91405 Orsay, France

Received: June 25, 2007; In Final Form: October 4, 2007

The performance of infrared (IR) spectroscopy of gas-phase ions in a commercially available 7 T Fourier transform ion cyclotron resonance mass spectrometer has been characterized. A π-allyl−palladium reactive intermediate, $[(\pi\text{-allyl})Pd(P(C_6H_5)_3)_2]^+$, involved in the catalytic allylation of amine is studied. A solution of this transition metal complex is electrosprayed, and the IR multiple photon dissociation (IRMPD) spectrum of the mass-selected ions is recorded in two spectral ranges. The fingerprint spectrum (650−1550 cm^{-1}) is recorded using the Orsay free-electron laser, and the dependence of the IRMPD efficiency on laser power and irradiation time is characterized. The DFT-calculated IR absorption spectrum of the $[(\pi\text{-allyl})Pd(P(C_6H_5)_3)_2]^+$ complex shows good agreement with the experimental spectrum. The π-interaction between the palladium and the allyl moiety is reflected by the assignment of the IRMPD bands, and the observed allylic CH_2 wagging modes appear to form a sensitive probe for the π-interaction strength in metal−π-allyl complexes. This spectral assignment is further supported by the analysis of the different IRMPD photofragmentation patterns observed at different photon energies, which are found to result from wavelength-specific photofragmentations. Nine peaks are well-resolved in the experimental spectrum, for which the bandwidth (fwhm) is on the order of 15 cm^{-1}. Resonances with a calculated IR intensity of 5 km/mol or larger are shown to be amenable for IRMPD, indicating an excellent sensitivity of our new experimental setup. Finally, the IR spectrum has also been recorded in the CH stretching region (2950−3150 cm^{-1}) using a tabletop IR optical parametric oscillator/amplifier (OPO/OPA) laser source.

1. Introduction

Electrospray ionization tandem mass spectrometry (ESI-tandem MS) has proven to be a powerful tool for analytical chemistry.[1] ESI-tandem MS traditionally derives structural information by fragmenting ions in the gas phase using a variety of activation methods.[2] The analysis of different aspects of structural properties of proteins in the gas phase, for instance, can be derived from the fragmentation of mass-selected ions either induced by collision-induced dissociation (CID) or through IR multiple photon dissociation (IRMPD) using a fixed wavelength CO_2 laser. More recently, electron capture dissociation (ECD) has been shown to provide a high fragmentation specificity toward the amide linkages of peptide backbones,[3−5] thus allowing for the determination of primary structure. In contrast to alternative heating methods, ECD preserves other features, such as the location of post-translational modifications.[3] Nevertheless, the potential for the 3D structural characterization of gas-phase molecular ions by tandem mass spectrometry could be dramatically enhanced by exploiting the recent developments associated with IR spectroscopy of mass-selected molecular ions.

The potential of combining IR lasers and tandem MS has been early realized, and the first combination of IR laser spectroscopy and a Fourier transform ion cyclotron resonance (FT-ICR) mass spectrometer was performed by the Beauchamp group using the narrow tuning range of a CO_2 laser.[6] Lee and co-workers were the first to use table-top pulsed lasers, tunable in the 3 μm wavelength range, to probe the OH stretches of ionic water solvated clusters;[7] the major areas of research initiated by this group are discussed in a recent review.[8] Due to the low density of molecular ions, resonant absorption is probed indirectly by monitoring the fragmentation efficiency of the molecular ion as a function of laser wavelength, and the resulting technique is often termed "action spectroscopy".[9,10] Most importantly, these pioneering studies demonstrated that high-fluence IR lasers can energize molecular ions in multiple photon absorption processes. The structure of molecular ions can thus be probed, even when they have a high fragmentation energy, using a spectroscopic technique now often referred to as IR multiple photon dissociation (IRMPD) spectroscopy.

The advent of free-electron lasers (FELs) as a tool for IR spectroscopy presented an opportunity to enlarge the spectral range in which IRMPD can be performed. These laser sources produce tunable mid-IR radiation in a broad wavenumber range, typically 100−2500 cm^{-1}, that covers the so-called molecular fingerprint region. Their high intensity make them very suitable for IRMPD spectroscopy. The first IRMPD experiments employing a FEL were performed on polyaromatic hydrocarbon cations[11] of astrophysical interest that were stored in a Paul trap; the combination of this ion trap with a FEL has been the subject of a recent review.[12]

To use the full potential of mass spectrometry, the first coupling[13,14] to an FEL of an FT-ICR mass spectrometer was realized at CLIO (Centre Laser Infrarouge d'Orsay).[15] A second experiment based on FT-ICR, installed at FELIX (Free Electron

* Corresponding author. Tel: +33-1-69-15-74-63. Fax: +33-1-69-15-61-88. E-mail: philippe.maitre@u-psud.fr.

[†] Present address: FOM Institute for Plasma Physics "Rijnhuizen", Postbus 1207, 3439 MN Nieuwegein, The Netherlands.

10.1021/jp074935e CCC: $37.00
Published on Web 12/05/2007

Laser for Infrared Experiments),[16] followed a year later.[17] These experiments enable the study of a large variety of molecular systems, ranging from organic[18−21] and organometallic[13,14,22−24] ions produced in situ by ion−molecule reactions to molecules of biological relevance brought out of solution into the gas-phase either by MALDI[25−27] or electrospray ionization (ESI).[28−33]

Fragmentation efficiency is a critical parameter to establish IRMPD spectroscopy as a routine activation method. In both home-built experiments based on FT-ICR mentioned above,[13,14,17] efficient fragmentation requires rather long irradiation times, often on the order of seconds. In contrast, irradiation for less than 50 ms can be sufficient to fragment all ions stored in a Paul ion trap,[33] where it seems that an efficient overlap between the (small) ion cloud and a tightly focused laser beam can be found. Under such conditions, the IRMPD signal can be observed for relatively weakly IR-active vibrational modes of molecular ions, when the FEL is on-resonance. In contrast, due to the larger ion cloud under FT-ICR conditions, the optimal focusing is the result of a subtle compromise between spatial overlap and laser intensity, which can demand long irradiation times needed to observe the finer details in an IRMPD spectrum.[33]

Here, we present a new experiment consisting of a commercially available 7 T FT-ICR mass spectrometer coupled to the CLIO FEL, as well as to an optical parametric oscillator/amplifier system. As a first experiment with this new setup, we present IRMPD spectroscopic measurements of a π-allyl−palladium complex. This study is part of our current project that aims at characterizing the reaction mechanism associated with the allylation of amine catalyzed by Pd(II) complexes. Allylation of amine involves the coupling of an amine and a C_3H_5X allylic substrate leading to the formation of a carbon−nitrogen bond. This coupling strongly relies on the presence of a good leaving group (X), allowing for an efficient formation of a transient π-allyl-metal complex. As a result, this reaction generally proceeds with substrates such as allylic carboxylates, carbonates, and phosphates.[34−36] An interesting challenge, from both an economical and an environmental point of view, would be to directly perform the reaction using allylic alcohol, and the search for efficient catalysts has become a major research objective.[37] Interestingly, it has recently been shown that allylation of amine using allylic alcohol can be efficiently catalyzed by π-allyl−palladium complexes without the necessity of adding an activating agent to enhance the leaving ability of the OH group.[38] It was suggested that the departure of the OH group is likely to be assisted by protonation resulting from a proton transfer from the Pd center to the hydroxyl group.[39] A key intermediate in this proposed mechanism would be the formation of the Pd−H moiety.[39] Several alternative catalytic mechanisms, with or without such a Pd−H reactive intermediate, have been investigated using ab initio quantum chemistry calculations.[40] In an attempt to better understand the successive elementary steps associated with the catalytic cycle, we currently perform a systematic study of a series of π-allyl−palladium catalysts by tandem MS and IR spectroscopy of reactive intermediates. As part of this project, we here present the IR spectra of a π-allyl−palladium cationic complex recorded in the 650−1650 and 2950−3150 cm^{-1} spectral ranges.

2. Experimental Section

The new experiment consists of a commercial 7 T FT-ICR mass spectrometer (Bruker, Apex Qe) and is schematically depicted in Figure 1. After electrospray ionization of a solution of the cationic complexes (10^{-5} M of $[(\pi\text{-allyl})Pd(P(C_6H_5)_3)_2]^+$ salt in tetrahydrofuran), ions are guided through a capillary and an ion funnel into a first hexapole ion trap, where they are collected for about 20 ms. One or multiple bunches of ions are then pulse-extracted into a ∼20 cm long RF quadrupole ion guide, where mass selection can be performed by resonant RF ejection of other species present. The quadrupole mass resolution is adjusted to transmit the full isotopic distribution of the parent π-allyl complex cation. Ions are then collected in a ∼5 cm long hexapole cell, where they are collisionally cooled using a flow of high-purity argon. A typical collection time for the current experiment in the hexapole collision cell is 500 ms, although in other experiments species are collected for periods as short as 1 ms. Ions are then pulse-extracted toward the ICR cell, where they are irradiated by IR light for a fixed time period. For each wavelength, the mass spectrum is the Fourier transform of a time-domain transient averaged three times.

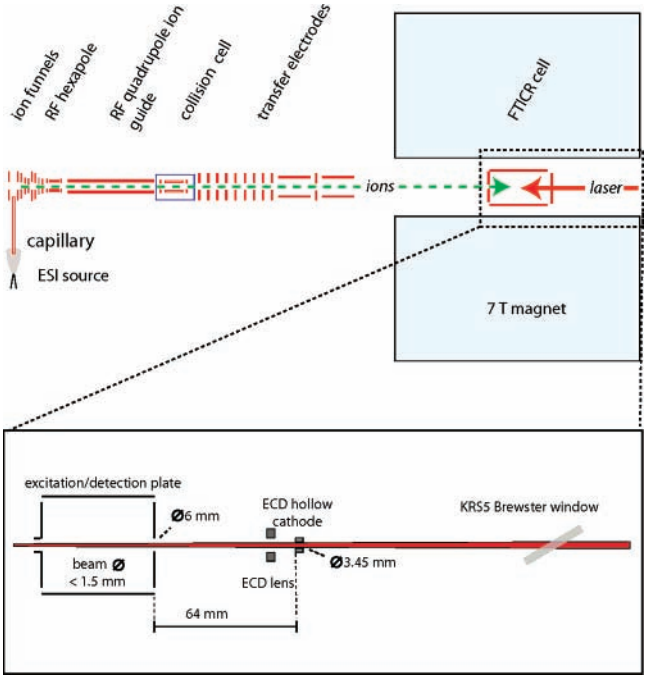

Figure 1. Schematic of the experimental instrument (top) and a detailed view of the ICR cell with the IR laser beam entering through a Brewster window (bottom).

The 63 mm long infinity ICR cell is placed inside the 155 mm diameter bore of a 7 T superconducting magnet (Magnex), and each trapping plate has a 6 mm diameter hole. Before entering the cell, the ions are decelerated by two ring electrodes of which the one closest to the trapping electrodes is segmented into two half-electrodes, allowing for a more efficient trapping by transferring longitudinal beam energy into transversal beam energy, the so-called "side-kick",[41] or for a correction of transversal beam energies. Some 50 mm beyond the second trapping electrode, a hollow cathode is placed to be used for ECD experiments. Electrons produced by this cathode can be focused into the trapped ion cloud using a ring electrode between the cathode and trapping electrode.

A 3.45 mm diameter aperture in the cathode allows for the IR laser beam to enter the cell. The IR light then traverses the ICR cell along the axis of the bore of the magnet in a single-pass configuration. The IR laser beam is loosely focused using a 2 m focal mirror and has a nearly constant diameter throughout the cell region.

IR spectroscopy in 650−1550 cm^{-1} wavenumber range was performed using the CLIO FEL, which produces pulsed, tunable IR light covering the 100−2500 cm^{-1} wavenumber range

(4−100 μm). The light is produced in an 8 μs long pulse train, the macropulse, of IR laser pulses a few picoseconds in duration, the micropulses. The macropulse repetition rate is 25 Hz while that of the micropulse is 62.5 MHz. Typical energies reached within one macropulse can be 40−60 mJ; for the current experiments, macropulse energies of ∼20 mJ are used.

The 2950−3150 cm^{-1} wavenumber range was explored using an IR optical parametric oscillator/amplifier (OPO/OPA) system of LaserVision, pumped by a 25 Hz Nd:YAG laser (Innolas Spitlight 600, 550 mJ per pulse, 4−6 ns pulse duration) at 1064 nm. In the presently covered wavenumber range, the typical output energy is ∼12 mJ per pulse. The spectral width of the laser is ∼5 cm^{-1}.

If the IR beam is in resonance with a strongly IR-active vibrational mode, light can be absorbed by the ions and the sequential absorption of several IR photons can lead to fragmentation of the mass-selected $[(\pi\text{-allyl})Pd(P(C_6H_5)_3)_2]^+$ ions. By recording the number of detected ions in the parent mass channel and that in the fragment mass channels while varying the wavelength of the IR light, an IRMPD spectrum is obtained. The IR-FEL photon energy was increased by steps of ∼2.5 cm^{-1}.

Density functional theory (DFT) calculations were performed to obtain the absorption spectrum of the π-allyl−palladium complex. All calculations were performed using the Gaussian 03 series of programs[42] using the B3LYP hybrid density functional. The basis set used for palladium is that of Hay and Wadt,[43] the one proposed for the small core quasirelativistic effective core potential, and a similar basis set quality was used for the other atoms.

3. Results: Photofragmentation Patterns and IR Spectra

3.1. Photofragmentation Patterns. The $[(\pi\text{-allyl})Pd(P(C_6H_5)_3)_2]^+$ ions are only mass-selected in the quadrupole ion guide placed before the hexapole collision cell, where they are accumulated for 500 ms before the transfer into the ICR cell; i.e., no mass selection is done in the ICR cell itself. Figure 2a (top) shows the mass spectrum recorded 1 s after the ion transfer into the ICR with the IR beam blocked. One can see in Figure 2a that there is only signal due to the parent ion, although a small third harmonic signal can also be observed. In the inset, an enlarged view of the parent ion mass spectrum is shown. Here, one can clearly observe the isotopic pattern characteristic of $[(\pi\text{-allyl})Pd(P(C_6H_5)_3)_2]^+$ ion with the most abundant isotope at *m*/*z* 671. In the following, we will only refer to the masses of the most abundant isotope.

Figure 2b shows the mass spectrum recorded when the mass-selected ions are irradiated for 1 s with the IR beam tuned to a resonance at 1092 cm^{-1}. A very efficient fragmentation of the parent ion into several mass channels can be observed, with the strongest fragmentation channel at *m*/*z* 409. Under all conditions where fragmentation is observed, the *m*/*z* 409 ion is the first fragment ion to appear, which is likely to result from the loss of a $P(C_6H_5)_3$ ligand. Five additional fragment ions are also observed in the mass spectrum displayed in Figure 2b. The analysis of the isotopic patterns at *m*/*z* 553, 409, 367, 333, 289, and 261 suggests that they correspond to $PdP_2C_{24}H_{19}^+$, $PdPC_{21}H_{20}^+$, $PdPC_{18}H_{14}^+$, $PdPC_{15}H_{14}^+$, $PdPC_{12}H_8^+$, and $PC_{18}H_{14}^+$, respectively. Mass spectra given in Figure 2c,d are recorded when the ions are irradiated for a longer period of time (10 s). When the IR laser is tuned to a resonance at 1442 cm^{-1} (Figure 2c), there is a nearly complete depletion of the parent ion (*m*/*z* 671), and the two *m*/*z* 261 and 289 ions are the most abundant fragments. Interestingly, these two fragment ions are not observed when the IR laser is tuned to a resonance at 1418 (Figure 2d), or at 948 cm^{-1} (not shown). As will be discussed below, these observations suggest that a wavelength-specific fragmentation might occur.

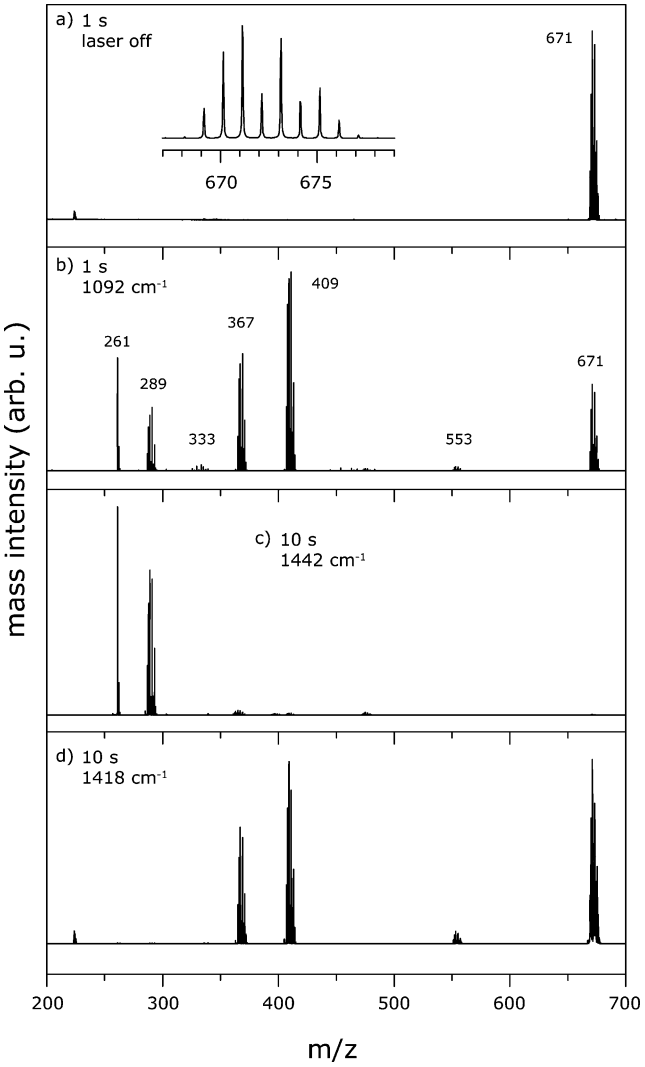

Figure 2. Mass spectra recorded following the transfer of the mass-selected $[((C_6H_5)_3P)_2(C_3H_5)Pd]^+$ π-allyl−palladium cationic complex in the ICR cell where they are stored for a period of 1 s. (a) When the laser is turned off, only *m*/*z* 671 is observed. A detailed view of the corresponding isotopic distribution characteristic of the parent ion is provided in the inset. (b) Multiple fragments are observed when the ions are irradiated for 1 s with the FEL tuned to 1092 cm^{-1}. (c and d) Mass spectra after irradiation for 10 s at 1442 cm^{-1} (d) and at 1418 cm^{-1} (d).

3.2. IR Spectra. If the wavelength is varied while recording the number of parent and fragment ions, an IRMPD spectrum is obtained. Two IRMPD spectra are given in Figure 3a,b, where the ordinate is the IRMPD efficiency defined as $-\ln[I_{par}/(I_{par} + \sum_i I_{frag,i})]$,[14] where I_{par} ($I_{frag,i}$) is the integrated intensity of the parent (*i*th fragment) ion. For these measurements, the ions are stored and irradiated in the ICR cell over a period of 250 ms or 2 s (Figure 3, parts a and b, respectively).

To aid in the interpretation of the recorded IRMPD spectra, DFT calculations are performed. The lowest-energy structure found displays a π-interaction between the allyl and the palladium in a pseudo-square-planar environment (Scheme 1). It is likely that other minima corresponding to different relative orientations of the phenyl groups exist on the potential energy surface. Nevertheless, the corresponding absorption spectra in the 650−1550 cm^{-1} spectral range should not differ significantly

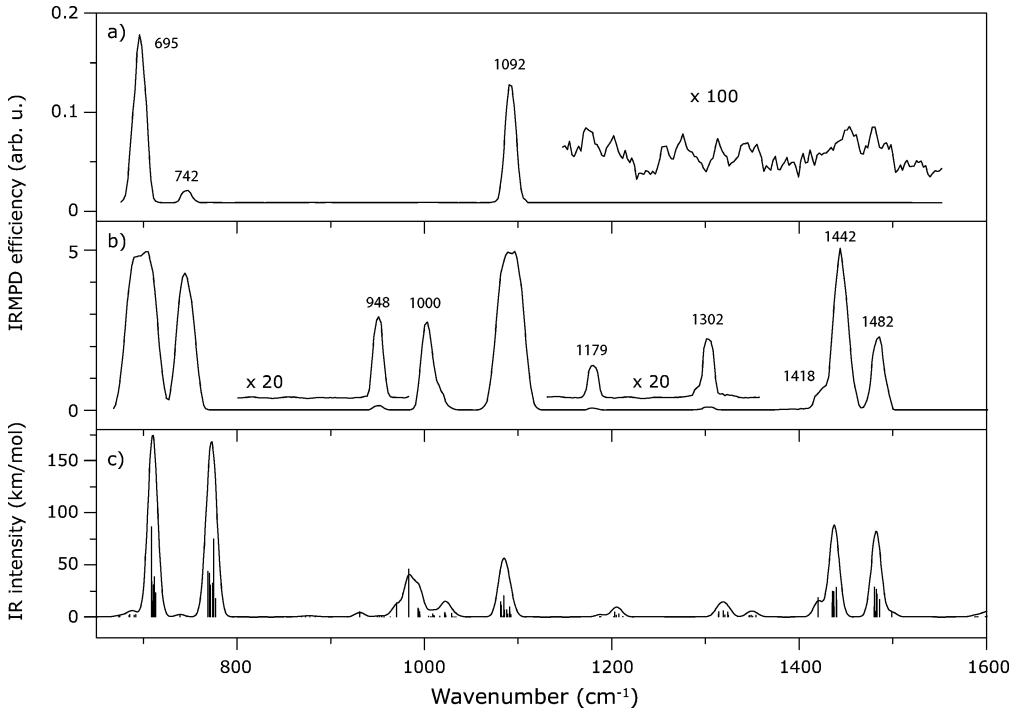

Figure 3. IR spectra of $[((C_6H_5)_3P)_2(C_3H_5)Pd]^+$ π-allyl−palladium cationic complex in the 650−1550 cm^{-1} range. (a and b) IRMPD spectra of mass-selected parent ions are recorded with irradiation periods of 250 ms (a) and 2 s (b). (c) Calculated IR absorption spectrum of the lowest energy structure of the $[((C_6H_5)_3P)_2(C_3H_5)Pd]^+$ parent ion. The calculated frequencies are scaled by 0.98, as are all of the frequency values noted in the discussion and Table 1. The calculated IR-active bands, given as sticks, are convoluted with a Gaussian line shape function with a Gaussian width of 10 cm^{-1}.

SCHEME 1: Optimized Structure of $[((C_6H_5)_3P)_2(C_3H_5)Pd]^+$

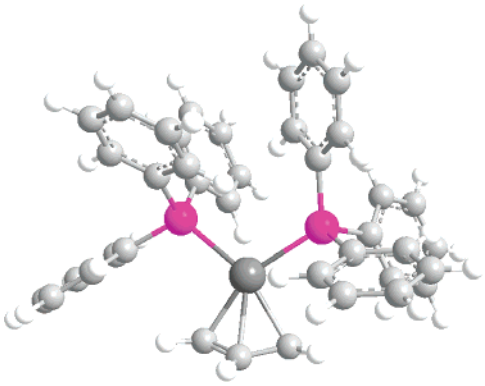

from that of the presently found structure. The calculated absorption spectrum is displayed in Figure 3c as a stick spectrum. The calculated frequencies are scaled by a factor of 0.98. Additionally, the spectrum is also shown convoluted with a Gaussian line shape function (10 cm^{-1} Gaussian width) representing the CLIO FEL spectral shape.

As can be seen in Figure 3, there is a quite good agreement between the positions of the calculated IR absorption bands and those of the IRMPD spectrum resulting from the irradiation of the ions for a period of 2 s. Although the observed relative intensities of the IRMPD bands differ from the relative calculated absorption intensities, the strongest IRMPD signals observed at 695, 742, 1000, 1092, 1442, and 1482 cm^{-1} nicely match with six strong maxima of the calculated IR absorption spectrum. Finally, it should be noted that the IRMPD band centered at 1442 cm^{-1} exhibits a shoulder at 1418 cm^{-1}, in good agreement with the convoluted calculated IR absorption spectrum.

Improving the resolution and the sensitivity of the IRMPD spectroscopy are two important aims for this new experimental setup. With the irradiation time of 2 s, bandwidths (fwhm) lower than 20 cm^{-1} are observed for the strong IRMPD bands at 742, 1000, 1442, and 1482 cm^{-1}. This resolution is similar to the one obtained when performing IRMPD spectroscopy with our quadrupole Paul ion trap coupled to the CLIO FEL,[33] which represents a significant improvement as compared to the resolution obtained with our lab-built FT-ICR. Under these conditions, it is also possible to observe rather weak IRMPD features: the observed resonances at 948, 1179, and 1418 cm^{-1} seem to be in good agreement with weak calculated absorption features of the $[(\pi\text{-allyl})Pd(P(C_6H_5)_3)_2]^+$ cation. However, this sensitivity comes at a cost. When the experimental conditions are such that IRMPD can be induced on-resonance with a weakly IR-active vibrational mode, saturation effects can be observed for vibrational modes with a larger IR cross section. The profiles of the IRMPD bands at 695 and 1092 cm^{-1} suggest that saturation occurs at these wavenumbers, which is reflected in their rather large bandwidths, 38 and 30 cm^{-1}, respectively. For these resonances, a complete depletion of the parent ion occurs when irradiated for 2 s. These observations are consistent with experiments on other molecular ions with large IR cross sections associated, for instance, with ether CO,[13] carbonyl CO,[14] or NO[20] stretches.

If the mass-selected *m/z* 671 ions are irradiated for only 250 ms, a better resolution of the two IRMPD features at 695 and 1092 cm^{-1} is obtained (Figure 3a). The bandwidth (fwhm) associated with the two strong IRMPD features is 14 and 10 cm^{-1} at 695 and 1092 cm^{-1}, respectively, thus significantly better than the ones obtained when the ions are irradiated for 2 s. In this case, the IRMPD spectrum is dominated by two strong features at 695 and 1092 cm^{-1}, with a weaker feature at 742 cm^{-1}. As can be seen in the inset of Figure 3a, the signal-to-noise ratio obtained after accumulating only three time-domain

TABLE 1: Experimental and Calculated Positions of the IR Bands $[((C_6H_5)_3P)_2(C_3H_5)Pd]^+$ Ions

ν_{exp} (cm^{-1})	ν_{calc} (cm^{-1})[a]	mode description
695	710	phenyl; out-of-plane CH bending
742	772	phenyl; out-of-plane CH bending
948	932	allyl; CH_2 rocking
1000	985	allyl; CH_2 wagging
1092	1073	phenyl; in-plane CH bending
1179	1191	phenyl; in-plane CH bending
1302	1305	phenyl; in-plane CH bending
1418[b]	1420[c]	allyl; asym CC stretch
1442	1423	phenyl; in-plane CH bending
1482	1467	phenyl; in-plane CH bending

[a] B3LYP harmonic values scaled by 0.98. [b] Shoulder on the red-side of the IRMPD band at 1442 cm^{-1}. [c] Calculated frequency of the asymmetric CC stretching mode of the allyl.

transient data is not sufficient for probing the IRMPD resonances in the 1400−1500 cm^{-1} spectral range. A more detailed analysis of the intensity dependence on experimental conditions is given in Section 4.3.

4. Discussion

4.1. Assignment of the IRMPD Bands. Considering the wavelength range (650−1550 cm^{-1}) explored in the present work, the probed vibrational modes of $[(\pi\text{-allyl})Pd(P(C_6H_5)_3)_2]^+$ complex should be the ones of the free ligands, shifted due to the interaction with the metal center. The frequencies of the observed IRMPD bands and those of the maxima of the calculated absorption spectrum of the lowest energy structure found for the $[(\pi\text{-allyl})Pd(P(C_6H_5)_3)_2]^+$ complex cation are given in Table 1. As can be seen in this table, there is a good agreement between theory and experiment.

The analysis of the normal modes reveals that the IR-active modes of the triphenylphosphine ligands strongly contribute to the IR spectrum in the 650−1550 cm^{-1} range. Out of the ten IRMPD bands observed for the $[(\pi\text{-allyl})Pd(P(C_6H_5)_3)_2]^+$ complex cation, seven can be assigned to phenyl vibrational modes of the triphenylphosphine ligand. As can be seen in Figure 3c, where the individual contributions of the IR-active modes of the complex are represented by sticks, maxima in the convoluted spectrum are often the result of the sum of the contributions of nearly degenerate IR-active vibrational modes. For instance, the maximum of the IR cross section at 772 cm^{-1}, which nicely matches with the position of the IRMPD band at 742 cm^{-1}, results from the sum of the nearly equally strong contributions of six out-of-plane CH bending vibrations, which closely resemble the ν_{11} vibrational mode of benzene.[44] Similarly, the two IRMPD bands at 1442 and 1482 cm^{-1} nicely match with two maxima of the calculated IR cross section at 1423 and 1467 cm^{-1}, respectively. Each of these two calculated bands results from six nearly degenerate in-plane CH bending modes of the phenyl groups, which closely resemble the ν_{19} mode of benzene.[44] Considering the bandwidth of the CLIO FEL, which is typically 0.5% of the central wavelength, it is likely that several IR-active modes might be simultaneously in resonance with the IR photons. This should significantly facilitate the absorption of multiple photons by the molecular ions.

IR-active vibrational modes of the allyl moiety may also contribute to the IRMPD spectrum. The analysis of the normal modes suggests that the two bands observed at 1000 and 948 cm^{-1} can be assigned to allyl vibrational modes (Table 1).

The IRMPD band observed at 1000 cm^{-1} is assigned to the two CH_2 wagging modes of the allyl. Calculated frequencies of the asymmetric and symmetric CH_2 wagging modes are 970 and 985 cm^{-1}, respectively. There are more IR-active modes in this energy range, as shown by the stick spectrum in Figure 3c, among which there are several phenyl vibrational (in-plane CH bending) modes. However, their IR intensities are predicted to be smaller than those of the asymmetric and symmetric wagging modes of allyl (14 and 46 km/mol, respectively). Moreover, the frequencies of the phenyl IR-active modes are predicted to be slightly higher than those of the two wagging modes of allyl, giving rise to an asymmetric shape for the calculated band; a similar asymmetric shape is observed for the IRMPD band at 1000 cm^{-1}.

The IRMPD band assigned to the CH_2 wagging modes may provide a signature of the π-interaction between the allyl and the palladium. Indeed, the position of the CH_2 wagging vibration has been shown to strongly depend on the bonding interaction between the allyl moiety and the metal center. In the case of σ-bound allyl (η^1 coordination), CH_2 wagging frequencies have been observed at higher frequencies (∼1100 cm^{-1})[45] than in the present case. In the case of $C_3H_5^-Na^+$, where the metal−allyl bond can be assumed to be ionic, the reported experimental frequencies for the two wagging modes are 888 and 917 cm^{-1}.[45] In the case of a π-allyl−palladium complex, $[(\pi\text{-allyl})PdCl_2]$,[45] the frequencies of the two CH_2 wagging modes associated with the η^3 coordinated allyl (945 and 963 cm^{-1})[45] are very close to the one determined for the presently studied π-allyl−palladium complex.

More generally, the observed frequency of out-of-plane CH bending modes of π-bonded unsaturated hydrocarbons, such as the ν_{11} mode of benzene,[44] has been shown to be a good diagnostic of the binding strength to a transition metal. Whereas most of the ligand modes are red-shifted upon coordination to a transition metal, out-of-plane CH bending modes have been shown to be blue-shifted. This shift seems to be due to the presence of the metal atom hindering the out-of-plane hydrogen bend. In the case of gas-phase cationic metal−benzene,[46] for example, the frequency of the out-of-plane CH bending mode could be compared to the one for the free ligand, and the ν_{11} benzene mode was shown to be blue-shifted by ∼100 cm^{-1} for $V^+(Bz)_2$. For the present case, the CH_2 wagging frequency for the neutral allyl radical (determined using matrix-isolation spectroscopy) was reported at 801 cm^{-1}.[47] One could thus conclude that the CH_2 wagging mode of allyl is significantly blue-shifted (∼200 cm^{-1}) in the $[(\pi\text{-allyl})Pd(P(C_6H_5)_3)_2]^+$ complex cation. Comparison to the neutral ligand, however, may not be appropriate in this case, since the coordinated allyl ligand is formally negatively charged. In this perspective, the $C_3H_5^-Na^+$ ionic complex may provide a better reference for evaluating the strength of the shift. Interestingly, the observed CH_2 wagging frequency for both the presently studied $[(\pi\text{-allyl})Pd(P(C_6H_5)_3)_2]^+$ (1000 cm^{-1}) and for $[(\pi\text{-allyl})PdCl_2]$ (945 and 963 cm^{-1})[45] appear significantly blue-shifted with respect to their position in $C_3H_5^-Na^+$ (888 and 917 cm^{-1}).

The weak IRMPD feature at 948 cm^{-1} seems to be purely associated with a rocking mode of the allyl CH_2 groups, since triphenylphosphine modes in this energy range have a very weak IR activity. The calculated intensity associated with the rocking mode of the allyl CH_2 groups is only 5.2 km/mol, and no calculated IR-active mode of appreciable oscillator strength is found within 20 cm^{-1}. All calculated resonances that are stronger than this have been observed. We thus derive that any resonance with a calculated IR intensity of 5 km/mol or larger is amenable for IRMPD. Of course, this is critically dependent on the, mostly unknown, fragmentation energies of the species

SCHEME 2: (a) A Possible Fragmentation Pathway of Mass-Selected $[((Ph)_3P)_2(C_3H_5)Pd]^+$ Ions (Ph = C_6H_5) Resulting in the Observed Mass Distribution and Proposed IRMPD Processes Occurring at 1442 cm^{-1} (b) and at 1418 cm^{-1} (c)[a]

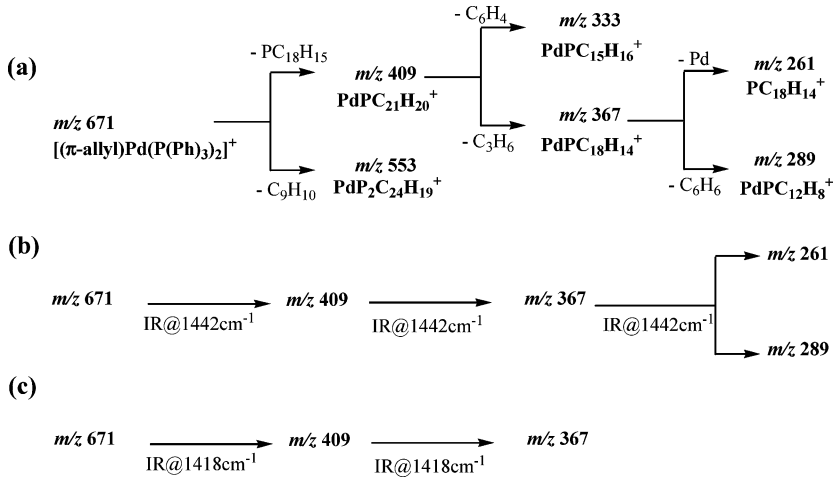

[a] These fragmentation pathways are based on MS4 experiments using an Esquire Paul trap experiment.

under study. However, it can be regarded as a rule-of-thumb for the sensitivity of our new experimental setup.

There are more IR-active modes of allyl; however, they are generally weaker than phenyl modes at similar frequencies, and their contribution is not likely to be large. There is one exception to this: the analysis of the IR-active modes in the 1400−1500 cm^{-1} wavenumber range strongly suggests that the shoulder on the red side of the IRMPD band at 1442 cm^{-1} can be assigned to the asymmetric C−C stretching mode of the allyl. The calculated intensity of this vibrational mode is significant (∼20 km/mol), and its calculated frequency is predicted to be ∼20 cm^{-1} lower than the IR-active phenyl modes contributing to the calculated band at 1442 cm^{-1}.

4.2. Wavelength-Specific Photofragmentation. The assignment of the observed IRMPD bands in the previous section has been based on the comparison with the calculated positions of the IR-active modes of the $[(\pi\text{-allyl})Pd(P(C_6H_5)_3)_2]^+$ complex cation. This assignment can be further supported by considering the photofragmentation patterns as a function of the IR laser wavenumber. As mentioned in the Results section, the photofragments observed following a long irradiation of the ions in the ICR cell (10 s) are quite different depending on whether the IR laser is tuned to 948 or 1418 cm^{-1} on the one hand or to 1442 cm^{-1} on the other. As can be seen in Figure 2 (c and d), the *m*/*z* 261 and 289 ions are observed at 1442 cm^{-1}, but not at 1418 cm^{-1}.

In order to understand these results, we will first consider the fragmentation pathways proposed in Scheme 2a. As mentioned in the Results section, it is likely that the *m*/*z* 409 fragment ion results from the loss of a $P(C_6H_5)_3$ ligand. Loss of the neutral C_6H_n is also observed in the mass spectrum of triphenylphosphine under electron impact ionization (70 eV) conditions.[48] Thus, it seems not surprising to observe a loss of neutral C_6H_4 from *m*/*z* 409 leading to the *m*/*z* 333 fragment ion. Loss of a neutral C_3H_6 could account for the formation of *m*/*z* 367 from *m*/*z* 409. Although no experiments with labeled compounds are performed, it is likely that neutral C_3H_6 results from the coupling of the allyl radical with an H atom. As a result, the $PdPC_{18}H_{14}^+$ *m*/*z* 367 ion could present a metallacycle similar to a reactive intermediate proposed in the "dissociative−associative" mechanism of C−H activation by cationic complexes.[49] A competitive fragmentation of the *m*/*z* 367 ion seems to occur, where a loss of Pd could lead to *m*/*z* 261 and a loss of (C_6H_6) could lead to *m*/*z* 289. Finally, the *m*/*z* 553 fragment corresponds to the loss of C_9H_{10}, which is likely to involve the departure of the allyl ligand and of a C_6H_n fragment from a triphenylphosphine ligand.

Both competitive and sequential fragmentations, such as the ones depicted in Scheme 2a, have already been observed when IR lasers are used to induce the fragmentation of molecular ions. We must recall that multiple IR absorption is generally believed to provide a slow activation process for molecular ions. One should thus expect a slow and stepwise increase of the internal energy of the ion until it is sufficiently high to overcome the lowest energy dissociation threshold. This has been recently evidenced, for example, by activating the furan radical cation using a CO_2 laser.[50] Nevertheless, competitive fragmentations have been observed in several cases such as $C_6D_6H^+$,[18] $Fe(CH_3OCH_3)_2^+$,[13] the *p*-aminobenzoyl cation,[51] or proton-bound dimers of alcohols,[52] for example. In a few particular cases,[51,52] variations of the branching ratio between two primary IRMPD photoproducts were characterized, but it should be stressed that these observations were made when molecular ions were irradiated under high fluence conditions using an IR-FEL on resonance with *very strongly* IR-active modes, such as a CO stretch,[51] or the asymmetric stretch associated with the proton shift between two alcohols.[52] When sequential fragmentation is observed, there is evidence that it occurs through a sequence of successive IRMPD processes. This has been clearly shown in the case of Fe^+(1-butene), for example, where bare Fe^+ ions were only observed when the CL10 FEL was simultaneously on resonance with IR-active modes of the Fe^+(1-butene) parent ion and of the Fe^+(butadiene) primary photofragment.[14,24]

A tentative rationalization of the wavelength-specific photofragmentation patterns can be made on the basis of the nature of the vibrational modes that are excited. As said above, even for long irradiation time (10 s) at 1418 cm^{-1} (Figure 2d) or 948 cm^{-1} (not shown), no photofragments are detected at *m*/*z* 261 and 289. In all cases where the photofragments *m*/*z* 261 and 289 are detected, phenyl vibrations are probed. In these cases, sequential fragmentation upon IR absorption as described above can take place, as long as the resulting fragment ions contain phenyl groups. However, if the vibration probed is localized in the allyl moiety, such a sequential process can come to a halt when the fragment ion no longer contains an allyl group. As can be seen in the fragmentation pathways proposed in Scheme 2a, the fragment at *m*/*z* 367 does not contain an allyl

group and therefore forms a natural terminus of the fragmentation process for allylic vibrational modes.

This wavelength-specific fragmentation behavior for different wavenumbers is not only inherently interesting but can also serve to confirm the vibrational assignment based on calculated IR absorption spectra (Table 1). Indeed, the weak IRMPD feature observed at 948 cm^{-1} seems to be purely due to IR absorption through CH_2 rocking mode of allyl, which is predicted to be weakly IR-active (5 km/mol). Similarly, the fragmentation patterns observed at 1418 cm^{-1} confirm that the shoulder on the red-side of the IRMPD band at 1442 cm^{-1} can be assigned to a vibrational mode of allyl.

Alternative explanations for this different fragmentation behavior can be considered. It can be argued that the resonances at 1418 and 948 cm^{-1} are fairly weak and that the absorbed energy available after irradiation over 10 s is insufficient to induce fragmentation of the *m*/*z* 367 fragment. However, for other comparably weak resonances, such as a phenyl mode at 1302 cm^{-1}, the *m*/*z* 261 and 289 are observed after 2 s of irradiation. More difficult to assess is the hypothesis that the vibrational structure of the fragment ions is different due to possible large structural rearrangements that could take place upon elimination of a fragment. A proper evaluation of this explanation would require experiments consisting of multiple isolation−irradiation steps. However, due to the favorable comparison between the experimental and calculated spectra, and particularly the fact that the fragmentation patterns are different *only* for allylic vibrations, it does not seem very likely.

4.3. IRMPD Efficiency. Under FT-ICR conditions, molecular ions experience complex trajectories.[53] Using our experimental setup based on a lab-built 1.25 T FT-ICR instrument, the spatial extent of the ion cloud was estimated to be on the order of ∼6 mm along the magnetic field axis and also ∼6 mm perpendicular to this axis;[33] these estimates were derived from the variations of the IRMPD efficiency of $Fe(CO)_5^+$ monitored as a function of the position of the laser beam waist along or perpendicular to the magnetic field axis, respectively. As already stated, the optimal focusing conditions are a compromise between a good spatial overlap with the ion cloud and a sufficiently high fluence to achieve multiple photon absorption. If the spatial overlap with the ions is incomplete, as was the case in the previous experiment, the temporal overlap between ions and laser macropulse becomes an important consideration. In the configuration of the home-built experiment, the IR beam traversed the cell in a direction *perpendicular* to the magnetic field. Since the ions have a large amplitude motion, the so-called "trapping motion", along the magnetic field axis and between the two trapping plates, with a period on the same order as the macropulse duration, ions may leave the interaction zone within the irradiation time, leading to a less efficient temporal overlap.

In the new configuration, where the IR laser beam traverses the cell *along* the magnetic field axis, incomplete temporal overlap due to the trapping motion is less likely to play a role and this should result in a better overall performance. As shown by the comparison of the IRMPD spectrum and calculated IR absorption spectrum given in Figure 3b,c, a good compromise in terms of efficiency and sensitivity was found with an IR laser beam focused with a 2 m focal mirror. Its diameter has been measured at different photon energies to be 1.37, 1.09, 0.86, and 0.66 mm at 1130, 1360, 1598, and 1832 cm^{-1}, respectively.

We also would like to insist on the fact that the so-called side-kick has an important effect on the IRMPD efficiency. The principle of the side-kick[41] is to reduce the ion translational energy along the magnetic axis and to convert it into cyclotron and magnetron energy. This is achieved by applying a small voltage, U_{sd} (of a few volts), over the segmented ring electrodes at the entrance of the ICR cell. This deflection voltage is likely to affect the overlap of the ion cloud with the IR beam. In the present experiment, the most efficient IRMPD conditions were obtained with a near-zero U_{sd} (within ±1 V). Furthermore, it was found that a change of U_{sd} on the order of ±1 V can be sufficient to fully deplete the IRMPD signal.

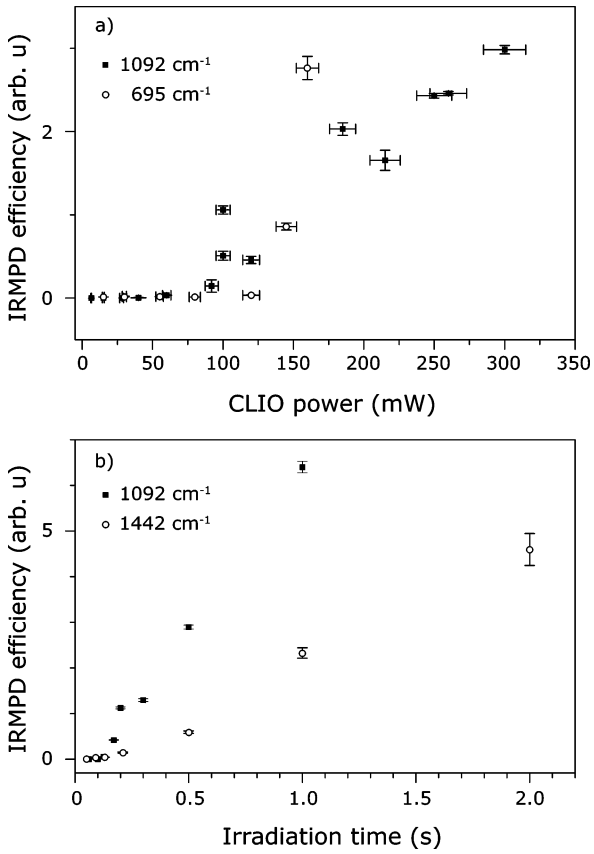

Figure 4. (a) IRMPD efficiency of $[((C_6H_5)_3P)_2(C_3H_5)Pd]^+$ π-allyl−palladium cationic complex as a function of laser power at 695 (squares) and 1092 cm^{-1} (circles). (b) IRMPD efficiency as a function of irradiation time at 1092 (squares) and 1442 cm^{-1} (circles), with constant laser power (∼700 and ∼400 mW, respectively).

In order to better characterize the performances of our experimental setup for the IR spectroscopy of molecular ions, the IRMPD efficiency as a function of irradiation time and laser power is studied, and the corresponding results are reported in Figure 4. The dependence of the IRMPD efficiency on (average) laser power has been investigated at two wavenumbers, 695 and 1092 cm^{-1}, and is displayed in Figure 4a. They have been recorded using fixed irradiation times, and the laser power is measured on the table before entering the FT-ICR cell. For the resonance at 1092 cm^{-1}, the IRMPD efficiency scales linearly with the laser power. It should be noted, however, that a nonlinear behavior is observed for laser powers below 100 mW when the FEL is tuned to 1092 cm^{-1}. For the data recorded at 695 cm^{-1}, linearity is not so obvious, as the macropulse energy obtained at this wavenumber did not allow for data at higher laser powers. A nonlinear fragmentation efficiency is observed for this resonance as well; the observation that fragmentation starts at higher powers could be due to the wavelength dependence of the laser beam diameter described above. The current observations are consistent with earlier IRMPD studies performed with our lab-built FTICR[14,31] and confirm that highly intense FEL laser sources are required for performing mid-

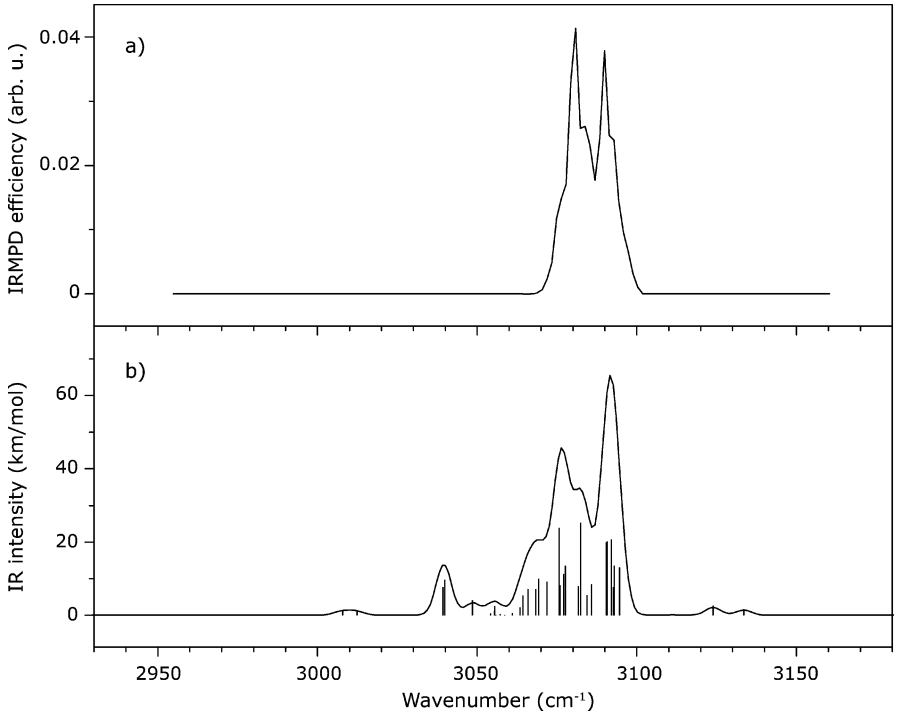

Figure 5. IR spectrum of $[((C_6H_5)_3P)_2(C_3H_5)Pd]^+$ π-allyl−palladium cationic complex recorded in the 2950−3150 cm^{-1} range with irradiation time of 1 s (a). The bottom spectrum (b) is the calculated IR absorption spectrum of the lowest energy structure of the $[((C_6H_5)_3P)_2(C_3H_5)Pd]^+$ parent ion. The calculated frequencies are scaled by 0.954. The calculated IR-active bands, shown as stick spectra, are convoluted with a Gaussian line shape function with Gaussian width of 5 cm^{-1}.

IRMPD spectroscopy on molecular ions with a relatively large (∼1 eV) fragmentation energy.

In an earlier experiment, the IRMPD efficiency of $Fe(CO)_5^+$ on resonance with a strongly IR-active vibrational mode (CO stretch) was found to scale linearly with the irradiation time.[14] Using the present experimental setup, the dependence of IRMPD efficiency on the irradiation time has been studied at two fixed photon energies (1092 and 1442 cm^{-1}) (Figure 4b). As can be seen in Figure 4, the IRMPD efficiency scales linearly with the irradiation time when the selected energy is 1092 or 1442 cm^{-1}, although there appears to be a nonlinear regime for the first few macropulses. This peculiar behavior may explain why a longer irradiation time is necessary for inducing the IRMPD phenomena, even on resonance with relatively strongly IR-active bands at 1000, 1442, and 1482 cm^{-1}.

4.4. Probing the CH Stretches in the 3000 cm^{-1} Energy Range. With the current sensitivity of gas-phase IR spectroscopy under our FTICR conditions using the CLIO FEL, it is appealing to find out under what conditions IRMPD spectroscopy can be performed using laser sources producing less intense radiation than the FEL. To this purpose, the IR spectrum of the $[(\pi\text{-allyl})\text{-}Pd(P(C_6H_5)_3)_2]^+$ complex cation has been recorded in the 2950−3150 cm^{-1} photon energy range using a tabletop IR OPO/OPA laser source. The coupling of an FT-ICR mass spectrometer with an IR OPO/OPA source has already been exploited by other groups for probing the structure of proton bound dimers of amino acids[54] and for deriving evidence for the transition from nonzwitterionic to zwitterionic structure of cationized arginine,[55] for example. In the present case, irradiation for 1 s on resonance with an IR-active mode of the *m*/*z* 671 parent ions exclusively leads to the formation of the *m*/*z* 409 primary fragment. Considering the relatively large binding energy of different alkylphosphines to Co^{II} derived for saturated (18-electron) (∼1.7−2.3 eV),[56] it is likely that formation of the *m*/*z* 409 ions by the loss of triphenylphosphine from the saturated (16 electron) $[(\pi\text{-allyl})Pd(P(C_6H_5)_3)_2]^+$ complex is induced by a multiple photon absorption process.

In the 2950−3150 cm^{-1} spectral range, the parent ions should display several IR-active bands associated with the CH stretching vibrations. The observed IRMPD spectrum is displayed in Figure 5a, together with the calculated IR absorption spectrum (Figure 5b). Two partly overlapping IRMPD bands are observed at 3075 and 3085 cm^{-1}. As can be seen in Figure 5, these two observed bands nicely match with the two strongest absorption features of the calculated absorption spectrum after scaling of the calculated frequencies by a factor 0.954. On the basis of the analysis of the normal modes, these two IRMPD bands can be assigned to phenyl CH stretches. Interestingly, the solution-phase IR absorption spectrum in the 3000 cm^{-1} region of triphenylphosphine is also dominated by two strong and partially overlapping bands at ∼3060 and ∼3080 cm^{-1}.[57] The CH stretching vibrations of the allyl moiety (calculated at ∼3010, ∼3040, and ∼3130 cm^{-1}) are only weakly IR-active (1−2 km/mol), and no photofragmentation signal is observed on resonance with these IR-active modes. The calculated intensities of the phenyl CH stretches are not extremely large (less than 25 km/mol). Nevertheless, as in the 650−1550 cm^{-1} range, the near degeneracy of several IR-active modes could significantly enhance the IRMPD process, since IR absorption could simultaneously occur through different vibrational modes.

Although a direct comparison between two such diverse laser sources is difficult, it is interesting to compare the IRMPD efficiency using the FEL and the IR OPO/OPA system. The observed IRMPD efficiency using the IR OPO/OPA is ∼0.05 after irradiation for 1 s at 3085 cm^{-1}. Interestingly, an IRMPD efficiency of 0.1 is observed after irradiation for 2 s for the resonance at 1302 cm^{-1}, for which the calculated IR intensity is very similar to that at 3085 cm^{-1}. In a forthcoming publication, we will report on a more in-depth study of IRMPD

spectroscopy of mass selected molecular ions using this IR OPO/OPA laser source.

5. Conclusions and Outlook

The performance of a new experimental setup for infrared spectroscopy of mass-selected molecular ions combining two laser sources covering a large spectral range with a commercially available 7 T FTICR has been presented. The structure of a π-allyl−palladium complex, $[((C_6H_5)_3P)_2(C_3H_5)Pd]^+$, a reactive intermediate involved in the catalytic allylation of amine, has been characterized. The spectroscopic resolution and sensitivity are notable for a system of this size and complexity. The IRMPD spectrum in the 650−1550 cm^{-1} spectral range recorded using the Orsay FEL presents nine clearly identifiable and well-resolved peaks, with a bandwidth on the order of 15 cm^{-1} (fwhm). It is deduced that IR-active modes with calculated intensities as low as 5 km/mol are amenable for IRMPD, thereby demonstrating a very efficient IRMPD process. With this current sensitivity, we also show that IR spectra can be recorded using laser sources producing less intense radiation than an IR FEL. The CH stretching region (2950−3150 cm^{-1}) of the IR spectrum has been recorded using an optical parametric oscillator/amplifier (OPO/OPA) system. The IRMPD efficiency as a function of irradiation time and laser power has been studied in order to better characterize the performances of our experimental setup for the IR spectroscopy of molecular ions. In the present case, an irradiation time on the order of 1 s is sufficient to reveal all the IR features of the π-allyl−palladium complex.

The IRMPD spectrum in the 650−1550 cm^{-1} spectral range compares favorably with a calculated spectrum obtained using density functional calculations, thus allowing for a clear assignment of the IRMPD bands. Two features (948 and 1000 cm^{-1}) are clearly associated with the allyl moiety, and the position of the band at 948 cm^{-1} is a clear signature of the π-interaction between the palladium and the allyl moiety. The photofragmentation patterns observed at different photon energies are clearly different. These observations are rationalized as resulting from wavelength-specific photofragmentation, depending whether the laser is on resonance with an allyl or a $P(C_6H_5)_3$ vibrational mode. The subsequent analysis further supports the spectral assignment of the IRMPD bands based on density functional calculations.

The present results confirm that tunable infrared lasers are particularly interesting for performing infrared multiple photon dissociation spectroscopy of mass-selected molecular ions in tandem mass spectrometers. The performances obtained for systems of the size and complexity as for the presently described transition metal complex are encouraging in the perspective of probing the structure of putative reactive intermediates associated with "real world" catalysts. This new experimental platform is under development in order to provide other ionization sources, such as a cluster source combined with a laser desorption−ionization source, besides the commercially provided ESI source. One of the principal goals of the new experiment is to combine the two mode-specific activation techniques mentioned above, ECD and resonant IRMPD, with high-resolution mass spectrometry to characterize the 3D structure of proteins and their noncovalent complexes.

Acknowledgment. We gratefully acknowledge the European Commission for a generous grant associated with the EPITOPES (Electron Plus Infrared TO Probe and Elucidate Structures, EC project #15637) funded through the NEST (New and Emerging Science and Technology) program of the sixth framework program. We would like to thank P. Le Floch and N. Mézailles for providing us with fresh catalysts.

References and Notes

(1) Fenn, J. B.; Mann, M.; Meng, C. K.; Wong, S. F.; Whitehouse, C. M. *Science* **1989**, *246*, 64.
(2) Sleno, L.; Volmer, D. A. *J. Mass Spectrom.* **2004**, *39*, 1091.
(3) Mirgorodskaya, E.; Roepstorff, P.; Zubarev, R. A. *Anal. Chem.* **1999**, *71*, 4431.
(4) McLafferty, F. W.; Fridriksson, E. K.; Horn, D. M.; Lewis, M. A.; Zubarev, R. A. *Science* **1999**, *284*, 1289.
(5) Zubarev, R. A.; Demirev, P. A. *J. Am. Soc. Mass Spectrom.* **1998**, *9*, 149.
(6) Woodin, R. L.; Bomse, D. S.; Beauchamp, J. L. *J. Am. Chem. Soc.* **1978**, *100*, 3248.
(7) Okumura, M.; Yeh, L. I.; Lee, Y. T. *J. Chem. Phys.* **1985**, *83*, 3705.
(8) Lisy, J. M. *J. Chem. Phys.* **2006**, *125*, 132302.
(9) Dunbar, R. C. *Int. J. Mass Spectrom.* **2000**, *200*, 571.
(10) Duncan, M. A. *Int. J. Mass Spectrom.* **2000**, *200*, 545.
(11) Oomens, J.; van Roij, A. J. A.; Meijer, G.; von Helden, G. *Astrophys. J.* **2000**, *542*, 404.
(12) Oomens, J.; Sartakov, B. G.; Meijer, G.; Von Helden, G. *Int. J. Mass Spectrom.* **2006**, *254*, 1.
(13) Maitre, P.; Le Caer, S.; Simon, A.; Jones, W.; Lemaire, J.; Mestdagh, H. N.; Heninger, M.; Mauclaire, G.; Boissel, P.; Prazeres, R.; Glotin, F.; Ortega, J. M. *Nucl. Instrum. Methods Phys. Res., Sect. A* **2003**, *507*, 541.
(14) Lemaire, J.; Boissel, P.; Heninger, M.; Mauclaire, G.; Bellec, G.; Mestdagh, H.; Simon, A.; Caer, S. L.; Ortega, J. M.; Glotin, F.; Maitre, P. *Phys. Rev. Lett.* **2002**, *89*, 273002.
(15) Prazeres, R.; Glotin, F.; Insa, C.; Jaroszynski, D. A.; Ortega, J. M. *Eur. Phys. J. D* **1998**, *3*, 87.
(16) Oepts, D.; Van der Meer, A. F. G.; Van, Amersfoort, P. W. *Infrared Phys. Technol.* **1995**, *36*, 297.
(17) Valle, J. J.; Eyler, J. R.; Oomens, J.; Moore, D. T.; van der Meer, A. F. G.; von Helden, G.; Meijer, G.; Hendrickson, C. L.; Marshall, A. G.; Blakney, G. T. *Rev. Sci. Instrum.* **2005**, *76*, 023103.
(18) Jones, W.; Boissel, P.; Chiavarino, B.; Crestoni, M. E.; Fornarini, S.; Lemaire, J.; Maitre, P. *Angew. Chem., Int. Ed.* **2003**, *42*, 2057.
(19) Chiavarino, B.; Crestoni, M. E.; Fornarini, S.; Lemaire, J.; Mac, Aleese, L.; Maitre, P. *Chemphyschem* **2004**, *5*, 1679.
(20) Chiavarino, B.; Crestoni, M. E.; Fornarini, S.; Lemaire, J.; Maitre, P.; MacAleese, L. *J. Am. Chem. Soc.* **2006**, *128*, 12553.
(21) Dopfer, O.; Lemaire, J.; Maitre, P.; Chiavarino, B.; Crestoni, M. E.; Fornarini, S. *Int. J. Mass Spectrom.* **2006**, *249*, 149.
(22) Le Caer, S.; Heninger, M.; Lemaire, J.; Boissel, P.; Maitre, P.; Mestdagh, H. *Chem. Phys. Lett.* **2004**, *385*, 273.
(23) Reinhard, B. M.; Lagutschenkov, A.; Lemaire, J.; Maitre, P.; Boissel, P.; Niedner-Schatteburg, G. *J. Phys. Chem. A* **2004**, *108*, 3350.
(24) Simon, A.; Jones, W.; Ortega, J. M.; Boissel, P.; Lemaire, J.; Maitre, P. *J. Am. Chem. Soc.* **2004**, *126*, 11666.
(25) Kapota, C.; Lemaire, J.; Maitre, P.; Ohanessian, G. *J. Am. Chem. Soc.* **2004**, *126*, 1836.
(26) Lucas, B.; Gregoire, G.; Lemaire, J.; Maitre, P.; Glotin, F.; Schermann, J. P.; Desfrancois, C. *Int. J. Mass Spectrom.* **2005**, *243*, 105.
(27) Lucas, B.; Gregoire, G.; Lemaire, J.; Maitre, P.; Ortega, J. M.; Rupenyan, A.; Reimann, B.; Schermann, J. P.; Desfrancois, C. *Phys. Chem. Chem. Phys.* **2004**, *6*, 2659.
(28) Polfer, N. C.; Oomens, J.; Dunbar, R. C. *Phys. Chem. Chem. Phys.* **2006**, *8*, 2744.
(29) Polfer, N. C.; Oomens, J.; Moore, D. T.; von Helden, G.; Meijer, G.; Dunbar, R. C. *J. Am. Chem. Soc.* **2006**, *128*, 517.
(30) Polfer, N. C.; Valle, J. J.; Moore, D. T.; Oomens, J.; Eyler, J. R.; Bendiak, B. *Anal. Chem.* **2006**, *78*, 670.
(31) Simon, A.; MacAleese, L.; Maitre, P.; Lemaire, J.; McMahon, T. B. *J. Am. Chem. Soc.* **2007**, *129*, 2829.
(32) Chiavarino, B.; Crestoni, M. E.; Fornarini, S.; Lanucara, F.; Lemaire, J.; Maitre, P. *Angew. Chem., Int. Ed.* **2007**, *46*, 1995.
(33) Mac Aleese, L.; Simon, A.; McMahon, T. B.; Ortega, J. M.; Scuderi, D.; Lemaire, J.; Maitre, P. *Int. J. Mass Spectrom.* **2006**, *249*, 14.
(34) Tsuji, J.; Takahashi, H.; Morikawa, M. *Tetrahedron Lett.* **1965**, *6*, 4387.
(35) Tsuji, J. *J. Synth. Org. Chem. Jpn.* **1999**, *57*, 1036.
(36) Sato, Y.; Yoshino, T.; Mori, M. *J. Organomet. Chem.* **2005**, *690*, 5753.
(37) Hsu, Y. C.; Gan, K. H.; Yang, S. C. *Chem. Pharm. Bull.* **2005**, *53*, 1266.
(38) Kinoshita, H.; Shinokubo, H.; Oshima, K. *Org. Lett.* **2004**, *6*, 4085.
(39) Ozawa, F.; Okamoto, H.; Kawagishi, S.; Yamamoto, S.; Minami, T.; Yoshifuji, M. *J. Am. Chem. Soc.* **2002**, *124*, 10968.
(40) Piechaczyk, O.; Thoumazet, C.; Jean, Y.; le Floch, P. *J. Am. Chem. Soc* **2006**, *128*, 14306.

(41) Caravatti, P. U.S. Patent No. 4,934,089, 1990.

(42) Frisch, M. J.; Trucks, G. W.; Schlegel, H. B.; Scuseria, G. E.; Robb, M. A.; Cheeseman, J. R.; Montgomery, J., J. A.; Vreven, T.; Kudin, K. N.; Burant, J. C.; Millam, J. M.; Iyengar, S. S.; Tomasi, J.; Barone, V.; Mennucci, B.; Cossi, M.; Scalmani, G.; Rega, N.; Petersson, G. A.; Nakatsuji, H.; Hada, M.; Ehara, M.; Toyota, K.; Fukuda, R.; Hasegawa, J.; Ishida, M.; Nakajima, T.; Honda, Y.; Kitao, O.; Nakai, H.; Klene, M.; Li, X.; Knox, J. E.; Hratchian, H. P.; Cross, J. B.; Bakken, V.; Adamo, C.; Jaramillo, J.; Gomperts, R.; Stratmann, R. E.; Yazyev, O.; Austin, A. J.; Cammi, R.; Pomelli, C.; Ochterski, J. W.; Ayala, P. Y.; Morokuma, K.; Voth, G. A.; Salvador, P.; Dannenberg, J. J.; Zakrzewski, V. G.; Dapprich, S.; Daniels, A. D.; Strain, M. C.; Farkas, O.; Malick, D. K.; Rabuck, A. D.; Raghavachari, K.; Foresman, J. B.; Ortiz, J. V.; Cui, Q.; Baboul, A. G.; Clifford, S.; Cioslowski, J.; Stefanov, B. B.; Liu, G.; Liashenko, A.; Piskorz, P.; Komaromi, I.; Martin, R. L.; Fox, D. J.; Keith, T.; Al-Laham, M. A.; Peng, C. Y.; Nanayakkara, A.; Challacombe, M.; Gill, P. M. W.; Johnson, B.; Chen, W.; Wong, M. W.; Gonzalez, C.; Pople, J. A. Gaussian Program Suite. In *Gaussian 03*; Gaussian, Inc.: Wallingford, CT, 2004.

(43) Hay, P. J.; Wadt, W. R. *J. Chem. Phys.* **1985**, *82*, 299.

(44) Nakamoto, K. *Infrared and Raman Spectra of Inorganic and Coordination Compounds*, 5th ed.; Wiley-Interscience: New York, 1997; Part B.

(45) Sourisseau, C.; Guillemert, J.; Pasquier, B. *Chem. Phys. Lett.* **1974**, *26*, 564.

(46) Jaeger, T. D.; van Heijnsbergen, D.; Klippenstein, S. J.; von Helden, G.; Meijer, G.; Duncan, M. A. *J. Am. Chem. Soc.* **2004**, *126*, 10981.

(47) Nandi, S.; Arnold, P. A.; Carpenter, B. K.; Nimlos, M. R.; Dayton, D. C.; Ellison, G. B. *J. Phys. Chem. A* **2001**, *105*, 7514.

(48) Stein, S. E., Director, NIST Mass Spec Data Center. Mass Spectra. In *NIST Chemistry WebBook, NIST Standard Reference Database Number 69*; Linstrom, P. J.; Mallard, W. G., Eds.; National Institute of Standards and Technology: Gaithersburg, MD, 2005.

(49) Plattner, D. A. *Int. J. Mass Spectrom.* **2001**, *207*, 125.

(50) Wu, G.; Stace, A. J. *Chem. Phys. Lett.* **2005**, *412*, 1.

(51) Oomens, J.; Moore, D. T.; Meijer, G.; von Helden, G. *Phys. Chem. Chem. Phys.* **2004**, *6*, 710.

(52) Fridgen, T. D.; MacAleese, L.; McMahon, T. B.; Lemaire, J.; Maitre, P. *Phys. Chem. Chem. Phys.* **2006**, *8*, 955.

(53) Marshall, A. G.; Hendrickson, C. L. *Int. J. Mass Spectrom.* **2002**, *215*, 59.

(54) Oh, H. B.; Lin, C.; Hwang, H. Y.; Zhai, H. L.; Breuker, K.; Zabrouskov, V.; Carpenter, B. K.; McLafferty, F. W. *J. Am. Chem. Soc.* **2005**, *127*, 4076.

(55) Bush, M. F.; O'Brien, J. T.; Prell, J. S.; Saykally, R. J.; Williams, E. R. *J. Am. Chem. Soc.* **2007**, *129*, 1612.

(56) Gengeliczki, Z.; Sztaray, B.; Baer, T.; Iceman, C.; Armentrout, P. B. *J. Am. Chem. Soc.* **2005**, *127*, 9393.

(57) Stein, S. E., Director, NIST Mass Spec Data Center. Infrared Spectra. In *NIST Chemistry WebBook, NIST Standard Reference Database*; Linstrom, P. J.; Mallard, W. G., Eds.; 2005; Vol. 2004.